NACA

APR 3 1947

RESEARCH MEMORANDUM

for the

Air Materiel Command, Army Air Forces

HIGH-SPEED AERODYNAMIC CHARACTERISTICS OF A 1/7-SCALE

MODEL OF THE NORTHROP YB-49 AIRPLANE

By Robert C. Robinson

Ames Aeronautical Laboratory
Moffett Field, Calif.

TECHNICAL
EDITING
WAIVED

NATIONAL ADVISORY COMMITTEE
FOR AERONAUTICS

WASHINGTON

MAR 24 1947

NATIONAL ADVISORY COMMITTEE FOR AERONAUTICS

RESEARCH MEMORANDUM

for the

Air Materiel Command, Army Air Forces

HIGH-SPEED AERODYNAMIC CHARACTERISTICS OF A 1/7-SCALE

MODEL OF THE NORTHROP YB-49 AIRPLANE

By Robert C. Robinson

SUMMARY

Tests were conducted to find the effects of compressibility on
the longitudinal stability and control of a 1/7-scale semispan
model of the Northrop YB-49 airplane. Lift, drag, pitching moment,
and elevon hinge moments were measured and are presented in graphi-
cal form. The results show that, due to a loss of lift on the out-
board portion of the wing, the longitudinal static stability
decreased rapidly as the Mach number increased above 0.725 and
for Mach numbers above 0.735 the model experienced a climbing
moment at positive lift coefficients. Also, longitudinal-control
effectiveness began to decrease at a Mach number of about 0.725.

INTRODUCTION

The Northrop YB-49 airplane is a jet-propelled modification
of the XB-35 airplane and is powered by eight TG-180 engines.
Extensive low-speed wind-tunnel tests of models of the XB-35
airplane have been reported in references 1 and 2, but, since
the jet-powered YB-49 will attain appreciably higher speeds, it
was considered desirable to test a model at high Mach numbers
in order to find the effects of compressibility on its longi-
tudinal stability and control. Accordingly, at the request of the
Air Materiel Command, U. S. Army Air Forces, a 1/7-scale semispan
model of the YB-49 airplane was tested in the Ames 16-foot high-
speed wind tunnel.

The half-span model was mounted with its plane of symmetry at
the wind-tunnel wall and with no supporting members inside the test
section. Lift, drag, pitching-moment, and elevon hinge-moments
were measured at several angles of attack and Mach numbers. This
report describes the effects of compressibility on the above

characteristics and on the effectiveness of the longitudinal-control surfaces.

MODEL

The model, furnished by Northrop Aircraft, Inc., was a modification of the XB-35 model used for the tests reported in reference 2. The structure of the model consisted of a steel box spar and plywood ribs covered with a plywood skin. All supporting members were outside the tunnel. Two control surfaces were provided, an elevon which extended from 38.2 to 75.9 percent of the semispan from the plane of symmetry, and a longitudinal trim flap which extended from 75.9 percent of the semispan to the wing tip. The elevon, which was equipped with an electrical strain gauge and a remote-control positioner, had an internally sealed balance, the chord of which was approximately 40 percent of the elevon chord aft of the hinge line. The airplane duct system was represented with the entrance built to scale and the total exit area to scale but made up of three jet tubes instead of four tubes as on the airplane. During these tests the ratio of duct entrance velocity to free-stream velocity was approximately 0.31. There were two vertical fins on the model, one just outboard of the jet tubes and the other on the inboard side of the jet tubes. Dorsal fins extended forward on the upper surface to the 10-percent-chord line. The fins can be seen in figure 1, which shows the model mounted in the 16-foot wind tunnel, and in figure 2 which is a drawing of the model. The more important dimensions of the half-span model are as follows:

Wing area of model, square feet 40.82

Span of model, feet 12.30

Wing chord at root, feet 5.36

Wing chord at tip, feet 1.33

Mean aerodynamic chord, feet 3.75

Sweepback of 25-percent-chord line, degrees 23.12

Dihedral of 25-percent-chord line, degrees 1.00

Twist about 25-percent-chord line, degrees washout 4.00

Airfoil section at root . . . . NACA 65(318)-019

Airfoil section at tip . . . . NACA 65,3-018

Elevon chord, percent wing chord (approx.) 18

Elevon span, feet 4.75

Elevon balance, percent of elevon chord aft of hinge
   line (approx.) 40

Mean of squared elevon chords, square feet 0.309

SYMBOLS

The symbols used in this report are defined as follows:

V free–stream velocity, feet per second

V_i indicated airspeed, knots

ρ mass density of air, slugs per cubic foot

q free–stream dynamic pressure $\left(\frac{1}{2}\rho V^2\right)$, pounds per square foot

M Mach number corrected for blockage due to the model
$$\left(\frac{V}{\text{speed of sound}}\right)$$

M_o uncorrected Mach number

S wing area, square feet

$M.A.C.$ mean aerodynamic chord, feet

$\overline{c_e^2}$ mean of the squared elevon chords, square feet

b_e span of elevon, feet

C_L lift coefficient $\dfrac{\text{lift}}{qS}$

C_D drag coefficient $\dfrac{\text{drag}}{qS}$

$C_{m_{c.g.}}$ pitching–moment coefficient $\left(\dfrac{\text{pitching moment about the center of gravity}}{qS\ M.A.C.}\right)$

C_{h_e} elevon hinge–moment coefficient $\left(\dfrac{\text{elevon hinge moment}}{q\ \overline{c_e^2}\ b_e}\right)$

α angle of attack of root chord corrected for jet–boundary
           effects, degrees

α_u uncorrected angle of attack of root chord, degrees

$\Delta\alpha$ angle of attack increment, degrees

ΔC_D drag coefficient increment

δ_e elevon deflection, degrees (Positive when trailing edge is down.)

δ_t longitudinal trim flap deflection, degrees (Positive when trailing edge is down.)

c.g.'   longitudinal center–of–gravity location for neutral stability, stick fixed, percent of M.A.C.

γ specific heat of air at constant pressure divided by specific heat of air at constant volume

CALIBRATION AND CORRECTIONS TO DATA

The dynamic pressure calibration used in these tests was obtained from a static pressure survey of the test section with the tunnel empty except for the survey apparatus, and the calibration was corrected for the blockage due to the model. As this correction was applied to the Mach number and to the dynamic pressure before the model tests, it was not necessary to correct the coefficients for a change in dynamic pressure as was done in reference 3, which discusses the method of calibration and the blockage corrections. The blockage correction was

$$M = M_O + M_O K \left[\frac{1 + \frac{\gamma-1}{2} M_O^2}{\left(\sqrt{1-M_O^2}\right)^3} \right]$$

where

$$K = 0.00637 + 0.0545\ C_D$$

Moments were computed about a center–of–gravity at 25 percent of the mean aerodynamic chord and on the root chord line. Corrections to the angle of attack and drag coefficient due to the jet boundary were calculated from the charts of reference 4 and applied to the data. The corrections were:

$$\Delta\alpha = 1.125\ C_L,\quad \text{degrees}$$

$$\Delta C_D = 0.0197\ C_L^2$$

RESULTS AND DISCUSSION

Lift and Longitudinal Stability

The effects of compressibility on the aerodynamic characteristics of the YB-49 model, as shown by the tests in the 16-foot high-speed wind tunnel, began to appear at a Mach number of about 0.70 and were marked at a Mach number of 0.775. Figure 3 shows curves of angle of attack, pitching-moment coefficient, and elevon hinge-moment coefficient against lift coefficient at four elevon angles for Mach numbers from 0.40 to 0.725. Vibration of the elevon prevented the measurement of hinge moments at higher Mach numbers, but by rigidly restraining the elevon at both ends it was possible to take force data up to a Mach number of 0.775. Lift and pitching-moment data with the elevon restrained are presented in figure 4. The variation of pitching-moment coefficient with lift coefficient in figure 4(a) shows longitudinal instability beginning at a lift coefficient of about 0.35 and a Mach number of 0.70. At higher Mach numbers the instability progresses to lower lift coefficients, being strong at a Mach number of 0.775 and zero lift. The lift-curve slope was also much reduced at a Mach number of 0.775. Tuft studies showed that the instability resulted from stalling of the outboard portion of the wing, while lift was maintained over a large area near the root. Figures 5 and 6 present tuft pictures for uncorrected angles of attack of 2° and 4°. It is apparent that at 2° the tip stall occurred between Mach numbers of 0.75 and 0.775, while at 4° it occurred between 0.725 and 0.75.

The variation with Mach number of lift coefficient, pitching-moment coefficient, lift-curve slope, and longitudinal stability is shown more clearly in figure 7. Curves of lift coefficient against Mach number are presented for constant angles of attack from -2° to 6° and pitching-moment coefficient against Mach number is presented for constant lift coefficients from -0.10 to 0.40. In the range of model attitudes covered, the Mach numbers of lift and pitching-moment divergence varied from about 0.72 to 0.675. The curves of pitching-moment coefficient against Mach number in figure 7 show a climbing moment at all positive lift coefficients for Mach numbers above 0.735 due to the loss of lift on the outboard part of the wing at the higher Mach numbers. Lift-curve slope and center-of-gravity position for neutral stability are shown for level-flight lift coefficients (160,000 lb gross weight) and zero pitching moment at altitudes of sea level, 25,000 feet, and 35,000 feet. At sea level the lift-curve slope reached a maximum of 0.094 per degree at a Mach number of 0.725 and then decreased rapidly with increasing Mach number as the outer portion of the wing stalled. The stick-fixed neutral point reached its most rearward position (34 percent of the M.A.C.) at a Mach number of 0.725 and then moved rapidly forward with increasing Mach number. At 25,000 foot altitude the variation

of lift-curve slope and neutral point with Mach number was little
different from that at sea level, but at 35,000 feet the breaks in
the curves occurred at a somewhat lower Mach number.

The variation of elevon angle and elevon hinge-moment coef-
ficient for balance with indicated airspeed is shown in figure 8
for three altitudes and three model conditions chosen to show the
effects of trim-flap deflection and boundary-layer transition on
the stability of the model. The curves show the presence of stick-
fixed stability over most of the speed range for all the conditions
shown except at the higher speeds where there is a small region of
instability followed by extreme stability. The extreme stick-fixed
stability at the higher Mach numbers is evidently due to the loss of
elevon effectiveness which is shown in a later figure. The effects
of trim-flap deflection on the variation of elevon angle for bal-
ance with airspeed varied with altitude. At sea level the main
effect was a reduction in stick-fixed stability, while at the higher
altitudes the stability was increased at the lower speeds, followed
by a region of reduced stability. At the highest speeds the effects
of the trim flap were small. Fixing the boundary-layer transition
on the upper surface at 15 percent of the chord had an effect
similar to that of the small deflection of the trim flap. The
variation of elevon hinge-moment with airspeed indicated stick-free
stability over the speed range covered in the test, and the stability
increased with increasing altitude. Deflection of the trim flap
affected the hinge-moment coefficient in much the same manner as it
did the elevon angle for balance. Fixing the boundary-layer transi-
tion at 15 percent of the chord on the upper surface decreased the
stick-free stability slightly over most of the speed range.

Longitudinal Control

Figure 9 presents the variation of pitching-moment coefficient
and elevon hinge-moment coefficient with elevon angle at constant
lift coefficients for Mach numbers from 0.40 to 0.725. Hinge
moments were not measured at Mach numbers high enough to show any
pronounced effects due to compressibility, however, for negative
elevon angles the curves show an increased negative value of
$\partial C_{h_e}/\partial \delta_e$ at a Mach number of 0.725, indicating the beginning of
a decrease in balance effectiveness. The variation of pitching-
moment coefficient with elevon angle for Mach numbers of 0.70 to
0.775, with the elevon rigidly restrained, is presented in
figure 10; and in figure 11 the effects of longitudinal-trim-flap
deflection on pitching-moment coefficient are shown. Elevon and
trim-flap effectiveness were measured from figures 9, 10, and 11
and are plotted against Mach number in figure 12. The data indi-
cate that at zero lift coefficient a rather rapid decrease in
elevon effectiveness began at a Mach number 0.725, while at a lift
coefficient of 0.4 an increase in effectiveness began between Mach
numbers of 0.65 and 0.70. However, these values are for zero

elevon deflection, and the curve of pitching-moment coefficient
against elevon angle for a lift coefficient of 0.4 at 0.725 Mach
number in figure 10 shows that at small elevon deflections the
effectiveness was reduced and it may be expected that the elevon
effectiveness will decrease rapidly as the Mach number increases
above M = 0.725. The trim flap also began to lose effectiveness
at a Mach number of 0.725.

Drag Characteristics

The variation of drag coefficient with lift coefficient for
several Mach numbers is presented in figure 13. The drag coeffi-
cient at zero lift and 0.40 Mach number (Reynolds number about
8.5×10^6) was 0.011 compared with 0.012 reported in reference 2
for a Mach number of about 0.12 and a Reynolds number of about
7.5×10^6.
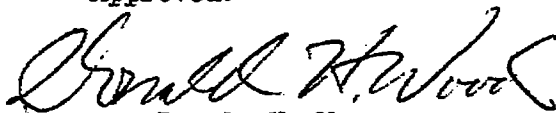
CONCLUSIONS

The results of tests of a 1/7-scale model of the YB-49 air-
plane in the Ames 16-foot high-speed wind tunnel led to the
following conclusions:

1. Static longitudinal instability began to appear at 0.70
Mach number and a lift coefficient of 0.35. At level-flight lift
coefficients the stability decreased rapidly as the Mach number
increased above 0.725.

2. The loss of lift on the outboard portion of the wing
resulted in a climbing moment for all positive lift coefficients at
Mach numbers above 0.735.

3. The effectiveness of both the elevon and the longitudinal
trim flap began to decrease with increasing Mach number at Mach
numbers between 0.70 and 0.725.

Ames Aeronautical Laboratory,
        National Advisory Committee for Aeronautics,
                Moffett Field, Calif..

                                                Robert C. Robinson

Approved: Robert C. Robinson,
                                                Aeronautical Engineer.

Donald H. Wood
        Donald H. Wood
Aeronautical Engineer.

REFERENCES

1. Sivells, James C., and Burgess, Jack: Tests in the NACA
     19-Foot Pressure Tunnel of a 1/10.75-Scale Model of the
     Northrop XB-35 Tailless Airplane. NACA CMR, Feb. 1943.

2. Teplitz, Jerome, Kayten, Gerald G., and Cancro, Patrick A.:
     Tests of a 1/7-Scale Semispan Model of the XB-35 Airplane
     in the Langley 19-Foot Pressure Tunnel. NACA CMR No.
     L5L27, 1946.

3. Nissen, James M., Gadeberg, Burnett L., and Hamilton,
     William T.: Correlation of the Drag Characteristics of
     a P-51B Airplane Obtained from High-Speed Wind-Tunnel
     and Flight Tests. NACA ACR No. 4K02, 1945.

4. Silverstein, Abe, and White, James A.: Wind-Tunnel Inter-
     ference with Particular Reference to Off-Center Positions
     of the Wing and to the Downwash at the Tail. NACA Rep.
     No. 547, 1935.

FIGURE LEGENDS

Figure 1.— The 1/7—scale semispan model of the YB—49 airplane
mounted in the Ames 16—foot high—speed wind tunnel. (a) Rear
view. (b) Front view.

Figure 2.— The 1/7—scale semispan model of the Northrop YB—49 airplane.

Figure 3.— The effects of elevon deflection on lift coefficient,
pitching—moment coefficient, and elevon hinge—moment coefficient.
1/7—scale YB—49 model. (a) M = 0.40.

Figure 3.— Continued. (b) M = 0.55.

Figure 3.— Continued. (c) M = 0.65.

Figure 3.— Continued. (d) M = 0.70.

Figure 3.— Concluded. (e) M = 0.725.

Figure 4.— The effects of elevon deflection on lift coefficient and
pitching—moment coefficient with the elevon rigidly restrained.
1/7—scale YB—49 model. (a) M = 0.70.

Figure 4.— Continued. (b) M = 0.725.

Figure 4.— Continued. (c) M = 0.75.

Figure 4.— Concluded. (d) M = 0.775.

Figure 5.— Tufts on the YB—49 semispan model. $\alpha = 2^o$.

Figure 6.— Tufts on the YB—49 semispan model. $\alpha = 4^o$.

Figure 7.— The effects of compressibility on lift coefficient,
pitching—moment coefficient, lift—curve slope, and longitudinal
stability. 1/7—scale YB—49 model.

Figure 8.— The variation of elevon deflection and elevon hinge—
moment coefficient with indicated airspeed for balance.
1/7—scale YB—49 model.

Figure 9.— The variation of pitching—moment coefficient and elevon
hinge—moment coefficient with elevon deflection. 1/7—scale
YB—49 model. (a) M = 0.4.

Figure 9.— Continued. (b) M = 0.55.

Figure 9.— Continued.   (c) M = 0.65.

Figure 9.— Continued.   (d) M = 0.70.

Figure 9.— Concluded.   (e) M = 0.725.

Figure 10.— The variation of pitching–moment coefficient with
     elevon deflection with the elevon rigidly restrained.
     1/7–scale YB–49 model.

Figure 11.— The variation of pitching–moment coefficient with
     trim–flap deflection. 1/7–scale YB–49 model. (a) M = 0.40.

Figure 11.— Continued.   (b) M = 0.65.

Figure 11.— Continued.   (c) M = 0.725.

Figure 11.— Concluded.   (d) M = 0.75.

Figure 12.— The effects of compressibility on the effectiveness
     of the elevon and the longitudinal trim flap. 1/7–scale
     YB–49 model. $\delta_e = 0^\circ$, $\delta_t = 0^\circ$.

Figure 13.— The variation of drag coefficient with lift coefficient
     at several Mach numbers. 1/7–scale YB–49 model.

(a) Rear view.

(b) Front view.

Figure 1.— The 1/7—scale semispan model of the YB—49 airplane mounted
in the Ames 16—foot high—speed wind tunnel.

12.30

9.52

4.86

4.80

2.92

LONGITUDINAL
TRIM FLAP

1.33

ELEVON

M.A.C.

5.36

₵ ROTATION

25 % CHORD LINE

3.145

23.12°

ALL   DIMENSIONS   IN   FEET

1° DIHEDRAL

FIGURE 2.- THE ½-SCALE SEMI-SPAN MODEL OF THE NORTHROP YB-49 AIRPLANE .

(a) M = 0.40

FIGURE 3.— THE EFFECTS OF ELEVON DEFLECTION ON LIFT COEFFICIENT,
PITCHING-MOMENT COEFFICIENT, AND ELEVON HINGE-MOMENT
COEFFICIENT. 1/7-SCALE YB-49 MODEL.

(b) M = 0.55

FIGURE 3.- CONTINUED. ¼ SCALE YB-49 MODEL.

(C) M = 0.65

FIGURE 3.—CONTINUED. 1/7-SCALE YB-49 MODEL.

(a) M = 0.70.

FIGURE 5.— CONTINUED. 1/16 - SCALE YB-47 MODEL.

(e) $M = 0.725$

FIGURE 3 - CONCLUDED. 1/7-SCALE YB-49 MODEL
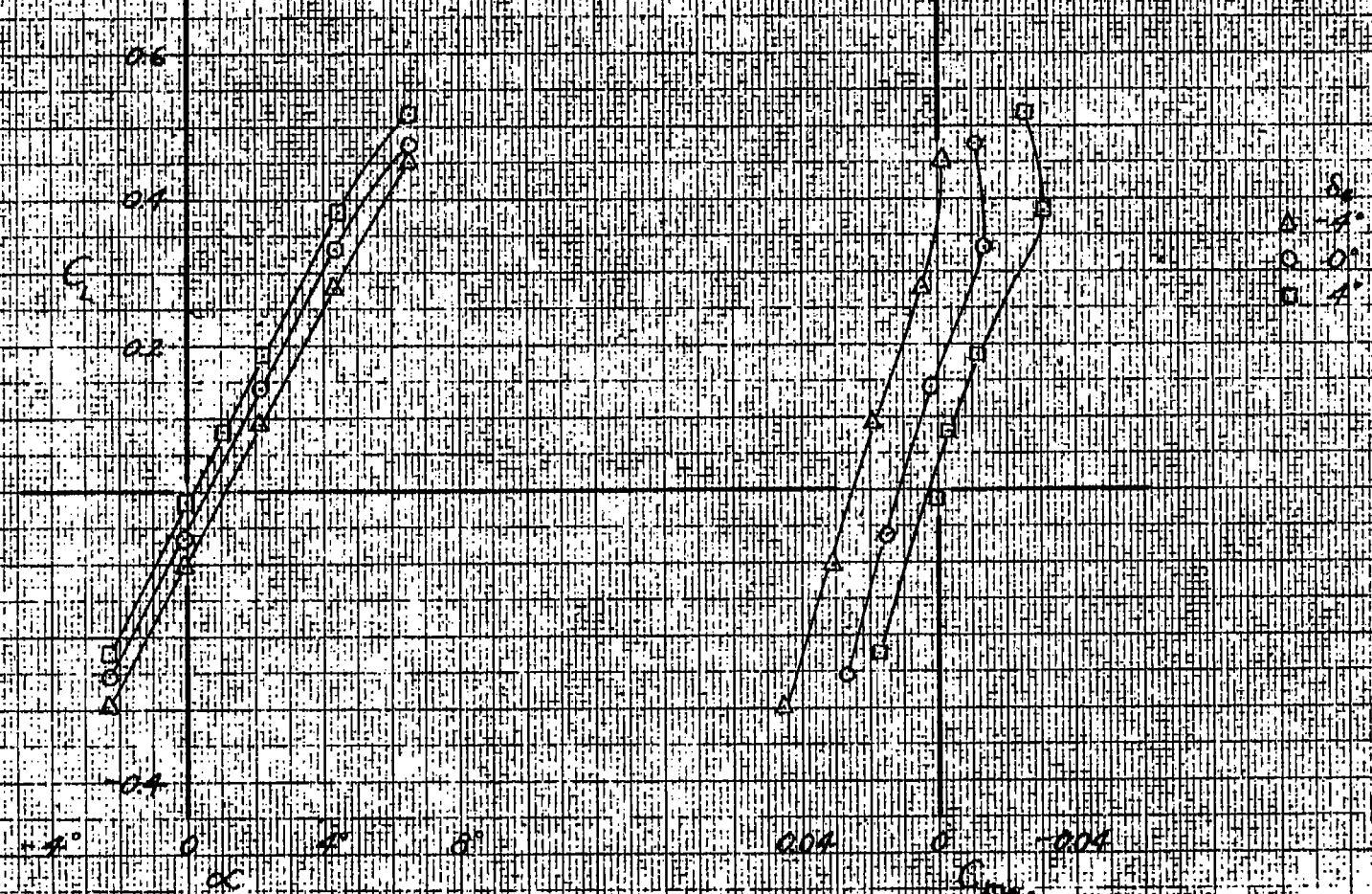
(a) M = 0.70

FIGURE 4.— THE EFFECTS OF ELEVON DEFLECTION ON LIFT COEFFICIENT
AND PITCHING MOMENT COEFFICIENT WITH THE ELEVON
RIGIDLY RESTRAINED. 1/1-SCALE XB-49 MODEL.

C_L

0.6

0.4

0.2

-0.4

4° 0 4° 8°

α

0.04 0 -0.04

$C_{m_{cg}}$

δ_e
△ -4°
○ 0°
□ 4°

(b) M=0.725

FIGURE 4.- CONTINUED. 1/7 - SCALE YB-49 MODEL.

C_L

0.6

0.4

0.2

0.2

0.4

-4°   0°   4°   8°

004   0   -004

α

$C_{mc.g.}$
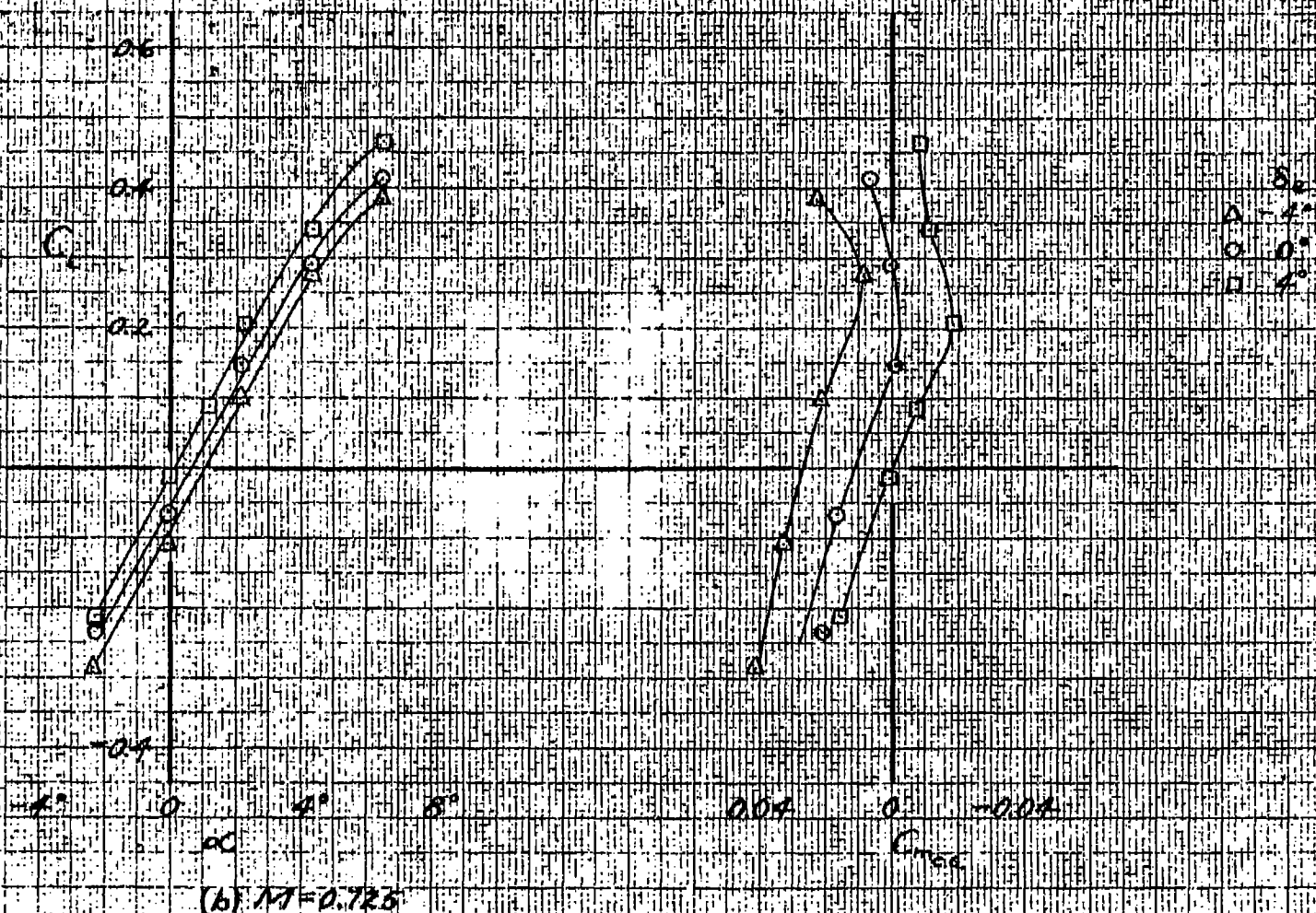
(c) M = 0.75

FIGURE 4- CONTINUED. 1/11 - SCALE YB-49 MODEL.
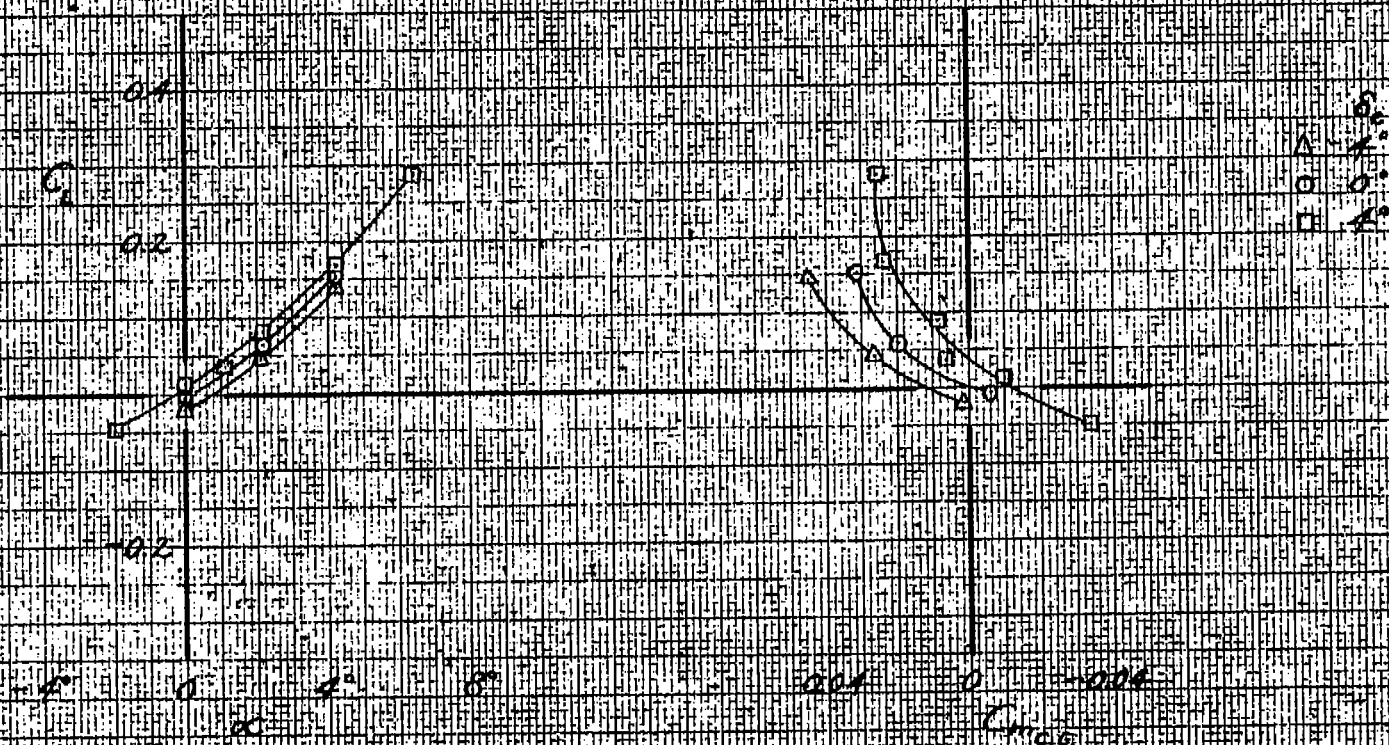
(d) M = 0.775

FIGURE 4.- CONCLUDED. 1/7-SCALE YB-49 MODEL.
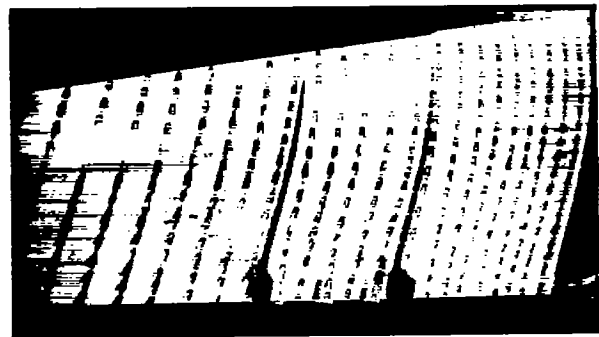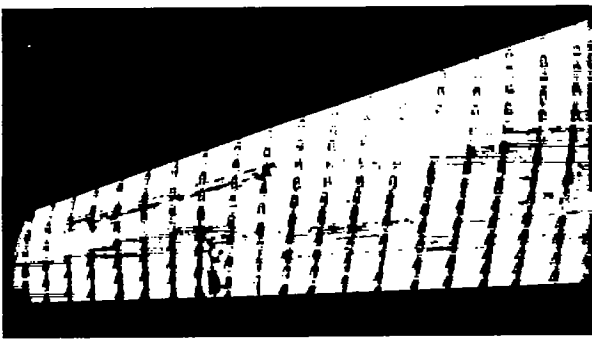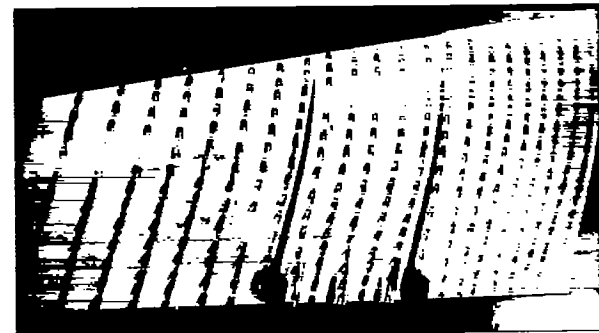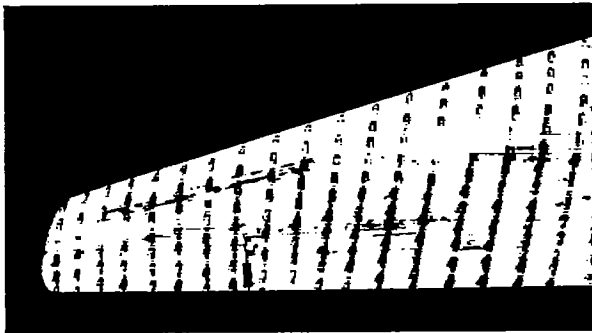
(a)   M = 0.725.

(b)   M = 0.75.
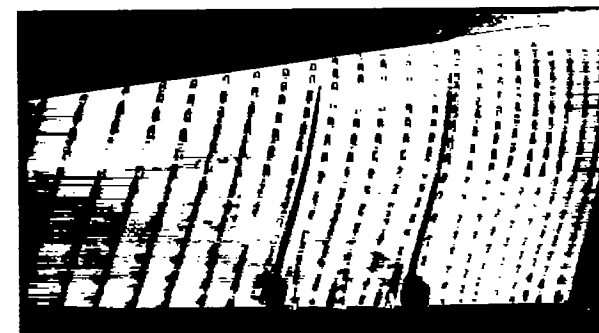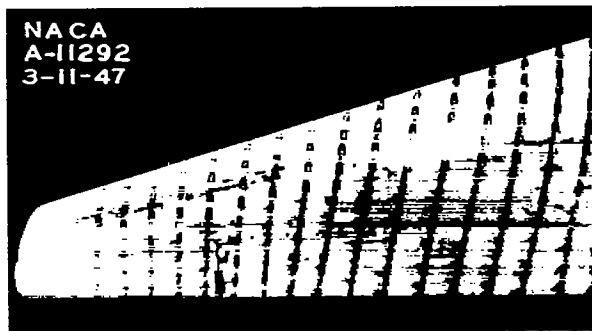
NACA
A-11292
3-11-47

(c)   M = 0.775.

Figure 5.— Tufts on the YB-49 semispan model.   α = 2°.
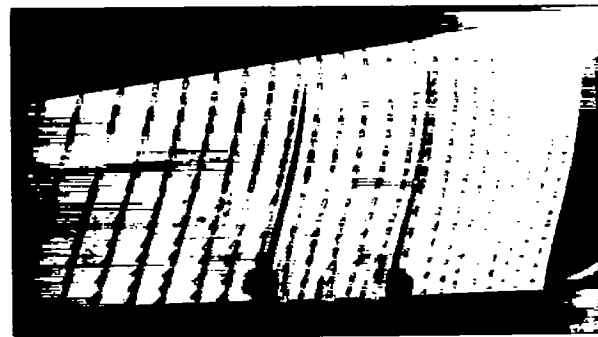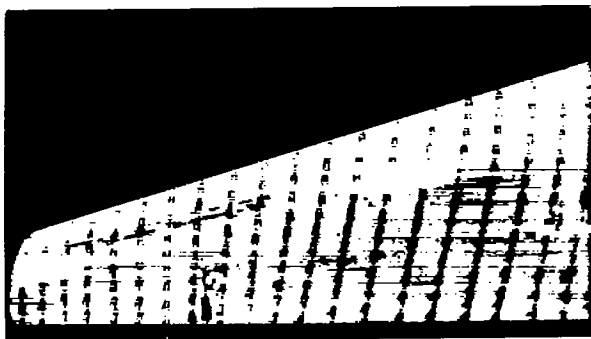
(a)　M = 0.70.
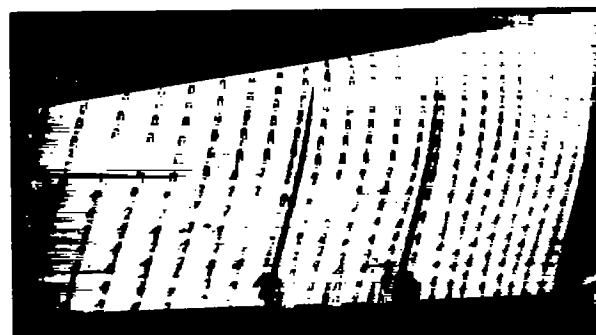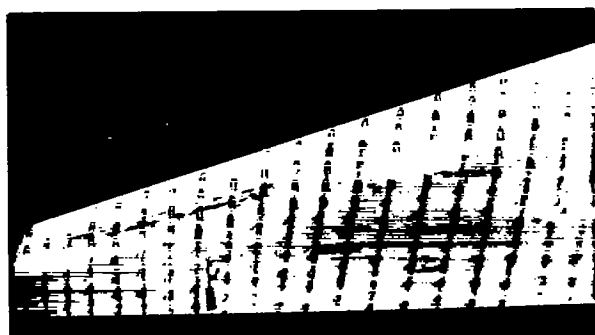
(b)　M = 0.725.

(c)　M = 0.75.

Figure 6.— Tufts on the YB—49 semispan model.　α = 4°.
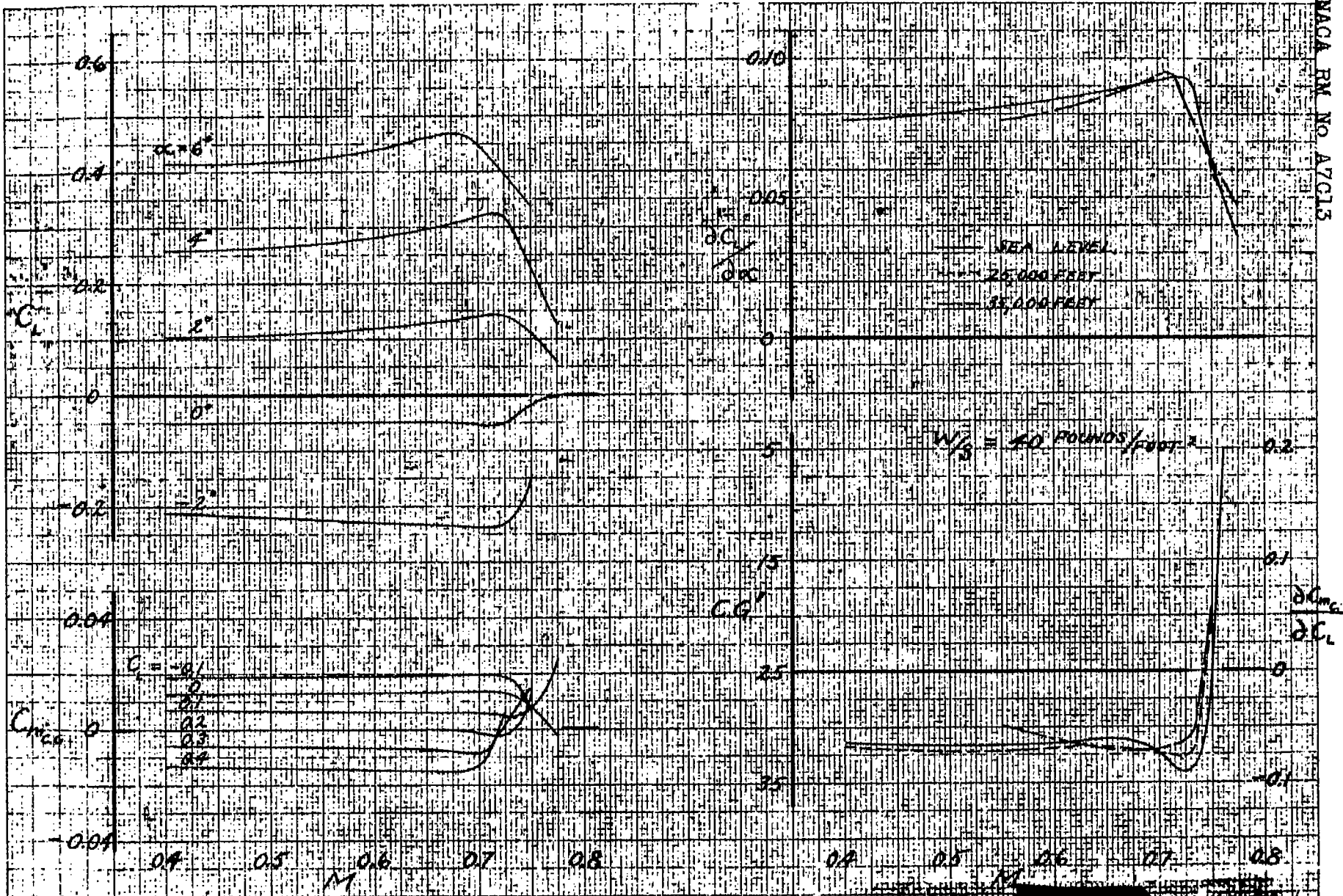
FIGURE 7.- THE EFFECTS OF COMPRESSIBILITY ON LIFT COEFFICIENT, PITCHING-MOMENT COEFFICIENT, LIFT-CURVE SLOPE, AND LONGITUDINAL STABILITY. 1/4 SCALE YB-49 MODEL
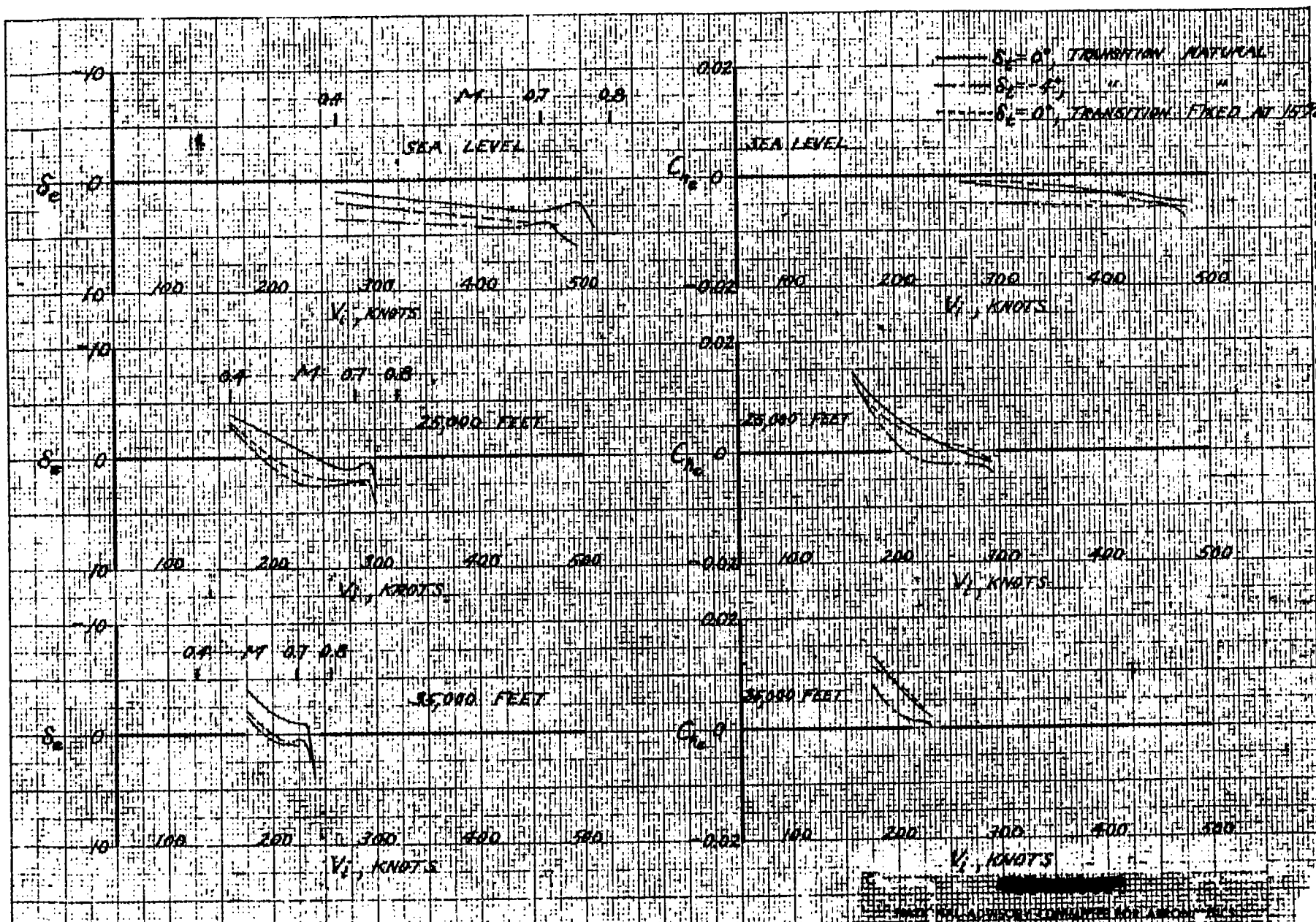
FIGURE 8.- THE VARIATION OF ELEVON DEFLECTION AND ELEVON HINGE - MOMENT COEFFICIENT WITH INDICATED AIRSPEED FOR BALANCE. 1/4-SCALE YB-49 MODEL
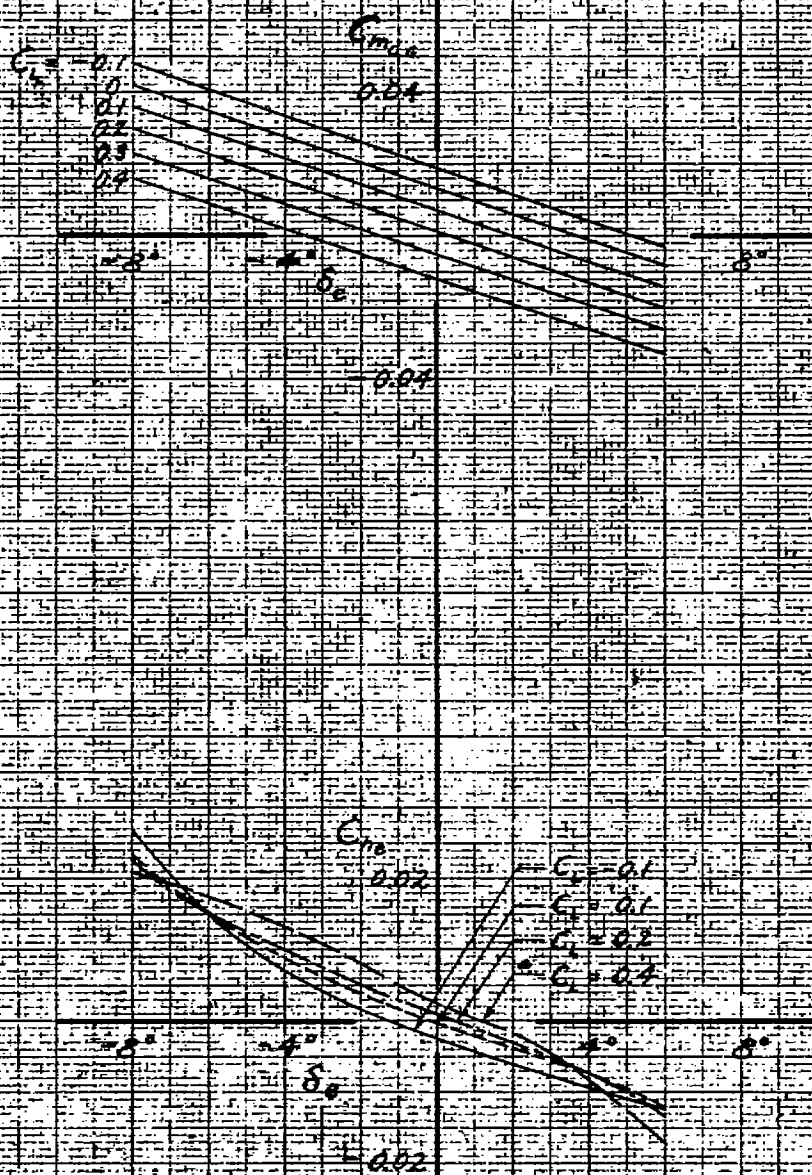
(a) M=0.4

FIGURE 9.— THE VARIATION OF PITCHING-MOMENT COEFFICIENT AND ELEVON HINGE-MOMENT COEFFICIENT WITH ELEVON DEFLECTION. 1/7-SCALE YB-49 MODEL.

(b) M = 0.55

FIGURE 9.— CONTINUED.   ¼-SCALE YB-49 MODEL.
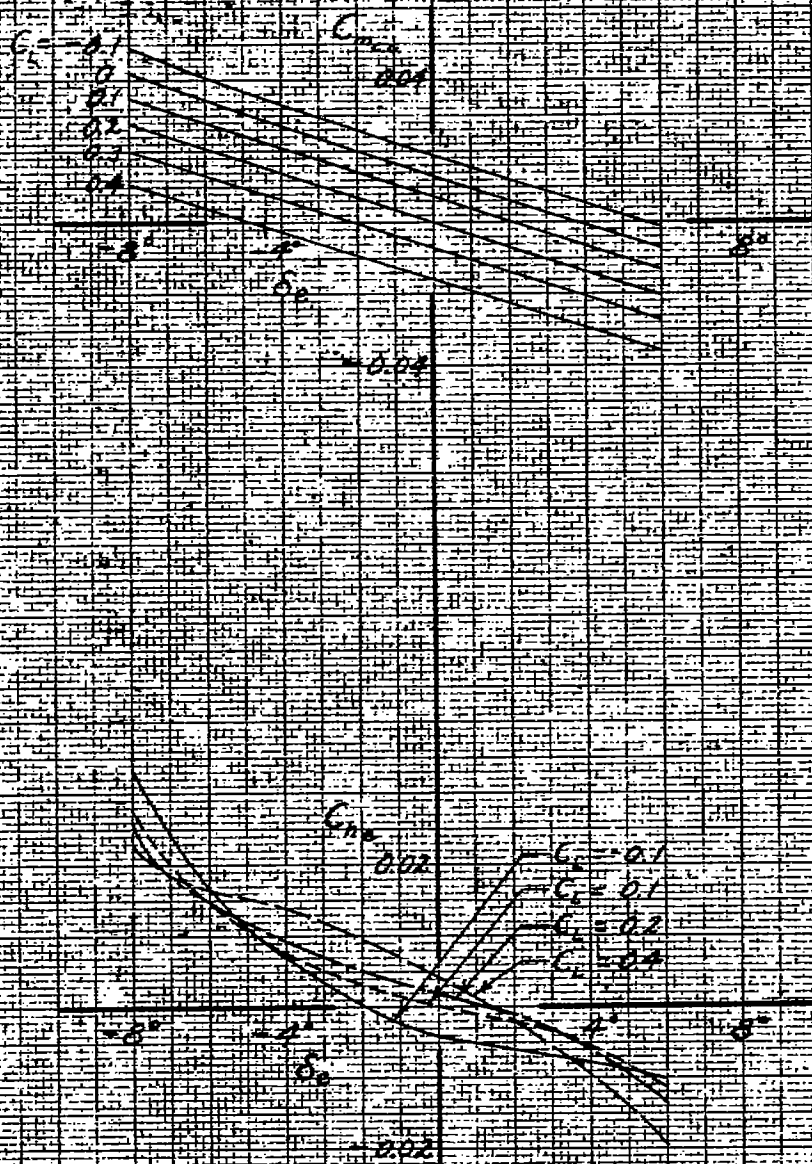
(C) M=0.65

FIGURE 9.- CONTINUED 1/4-SCALE YB-49 MODEL.
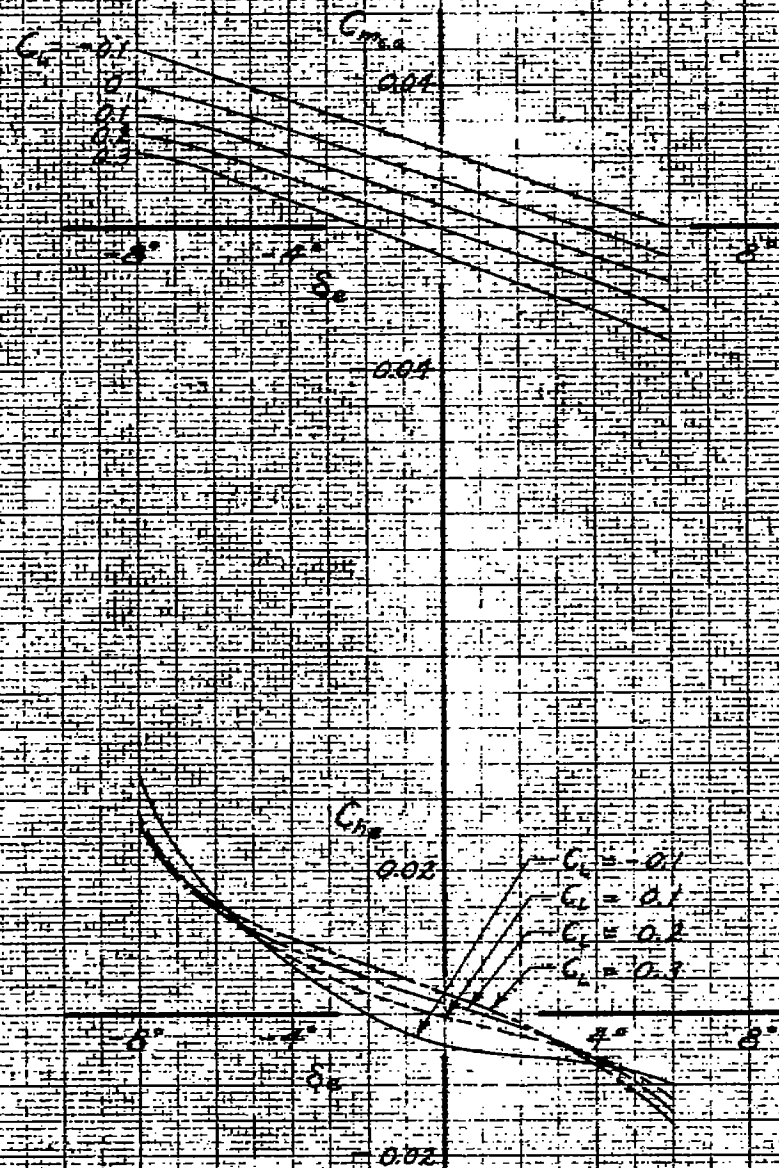
(d) M = 0.70

FIGURE 9.- CONTINUED 1/4-SCALE YB-49 MODEL.
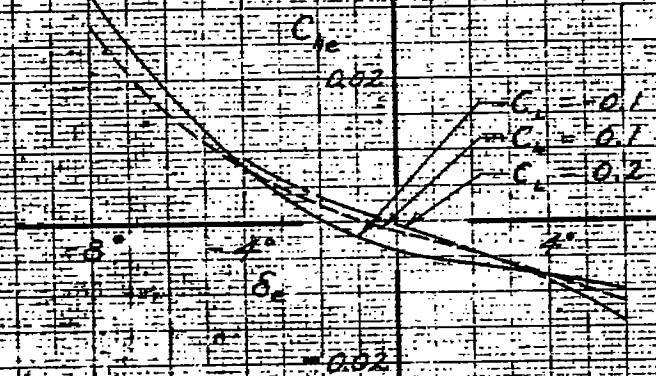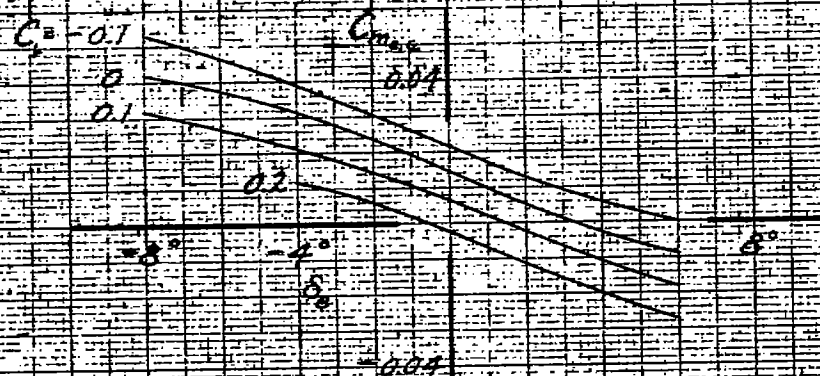
(e) $M = 0.725$

FIGURE 9 - CONCLUDED. $\frac{1}{7}$ - SCALE YB-49 MODEL
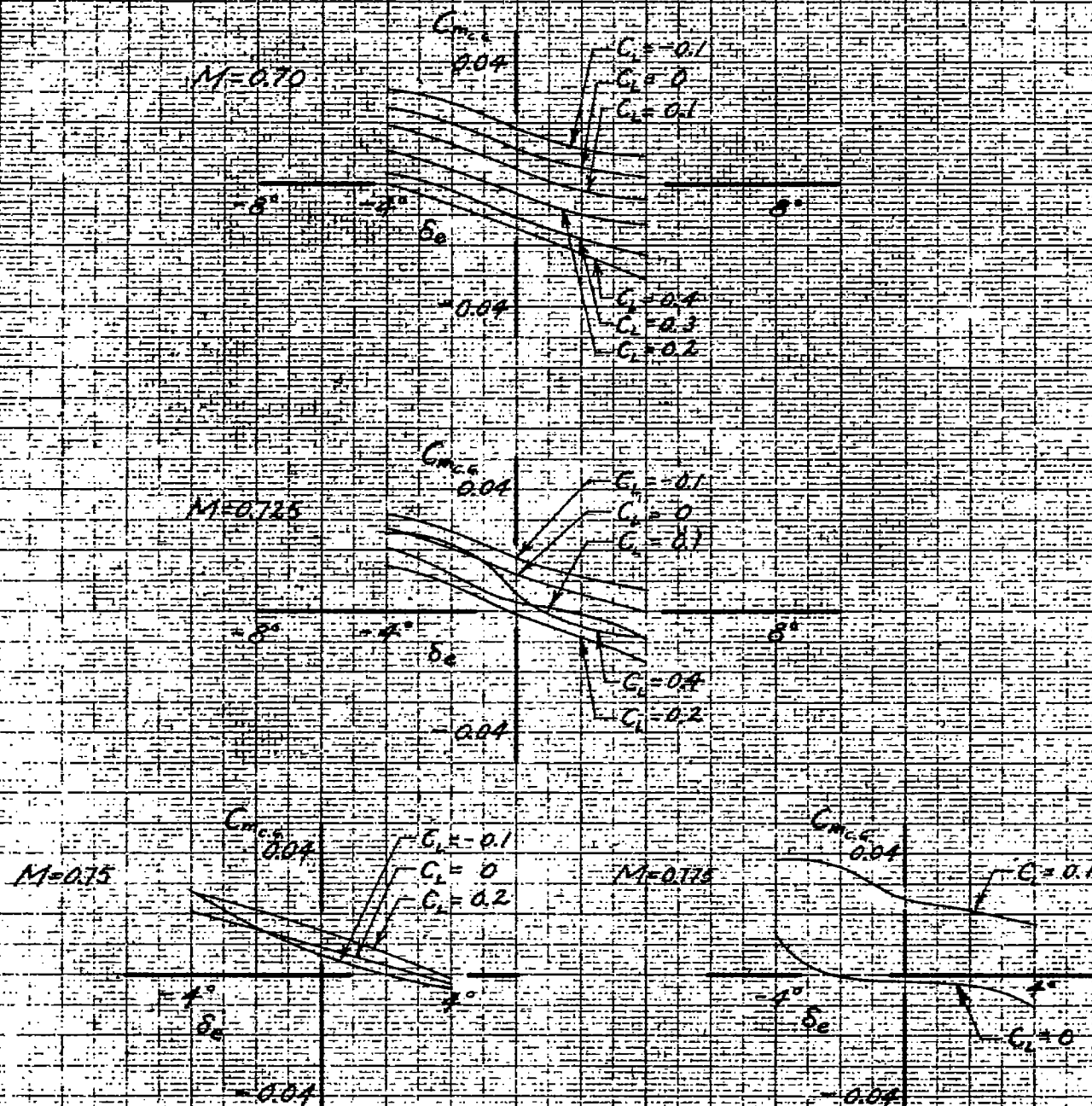
FIGURE 10.- THE VARIATION OF PITCHING-MOMENT
COEFFICIENT WITH ELEVON DEFLECTION WITH
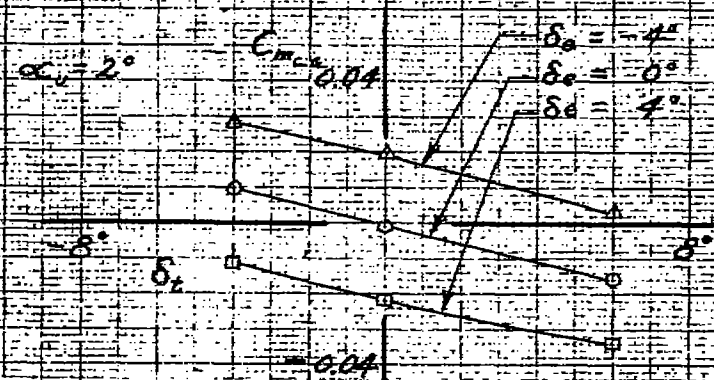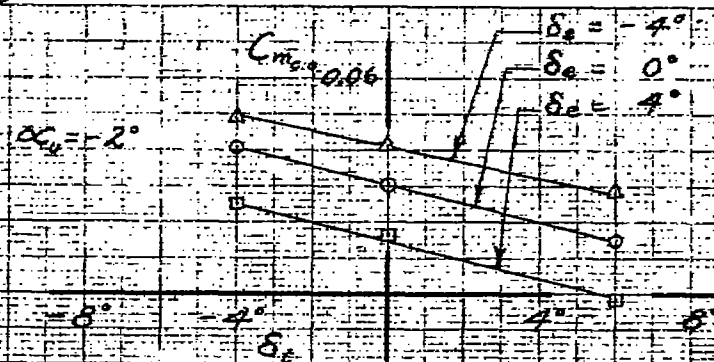THE ELEVON RIGIDLY RESTRAINED. 1/7 -SCALE
YB-49 MODEL.
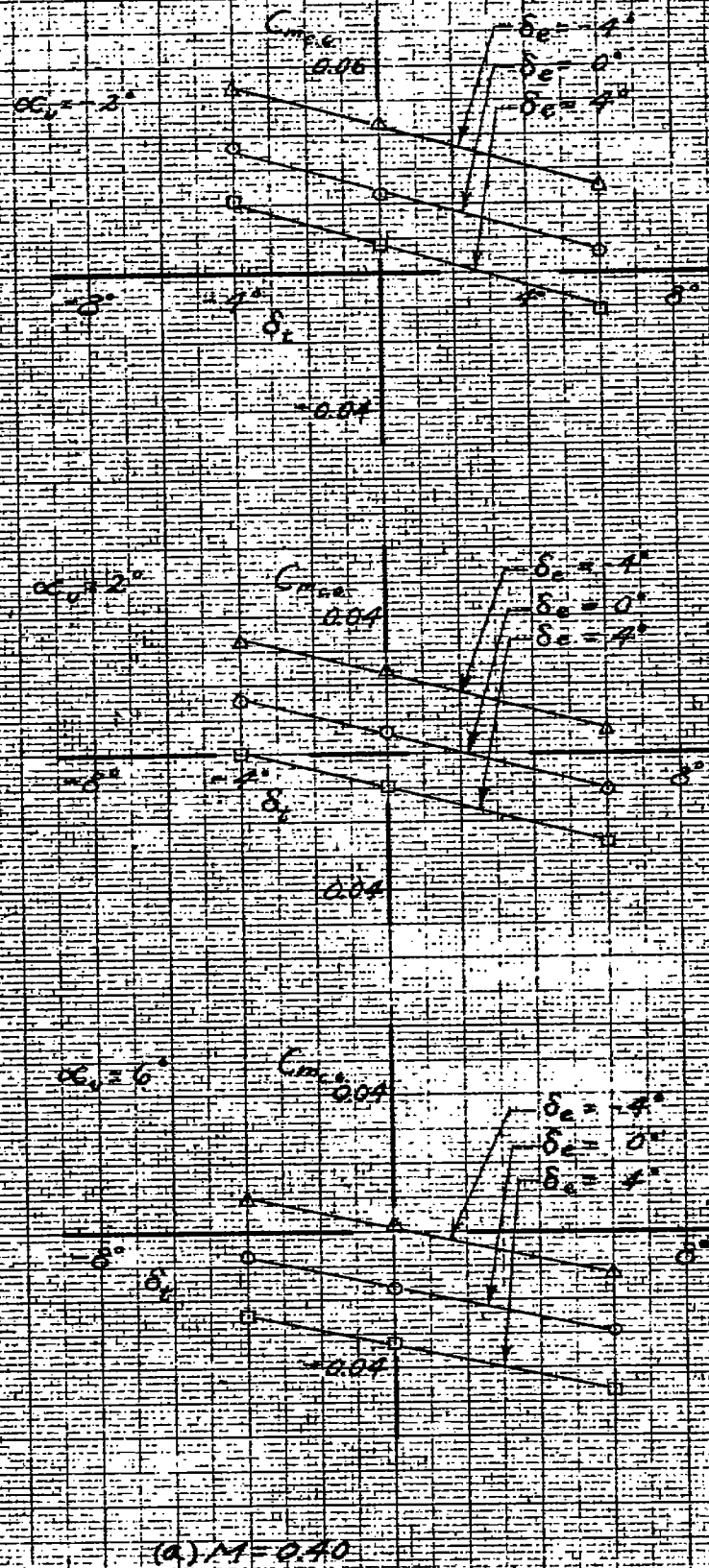
(a) M = 0.40

FIGURE 11.— THE VARIATION OF PITCHING-MOMENT
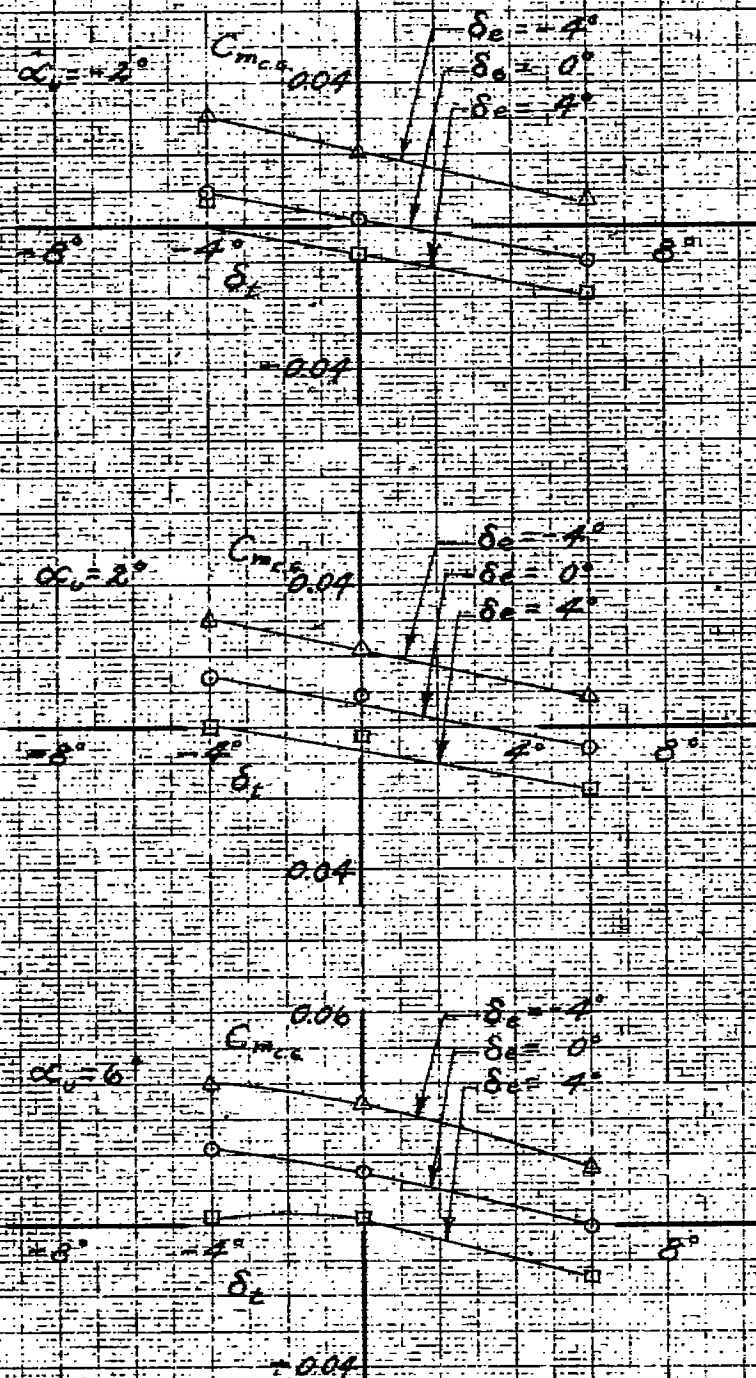COEFFICIENT WITH TRIM-FLAP DEFLECTION.
1/7 SCALE YB-49 MODEL
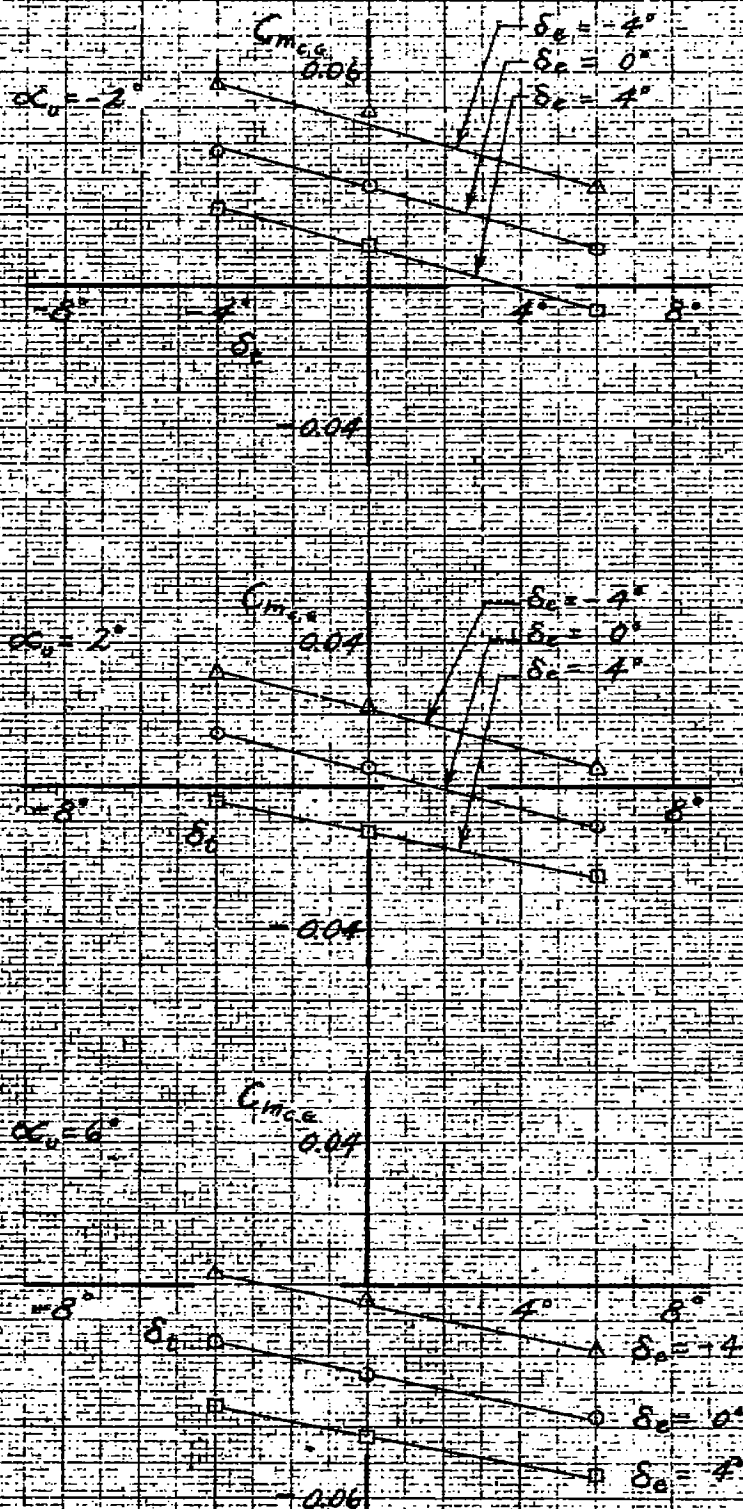
(b) M=0.65

FIGURE 11 - CONTINUED. 1/7 SCALE YB-49 MODEL
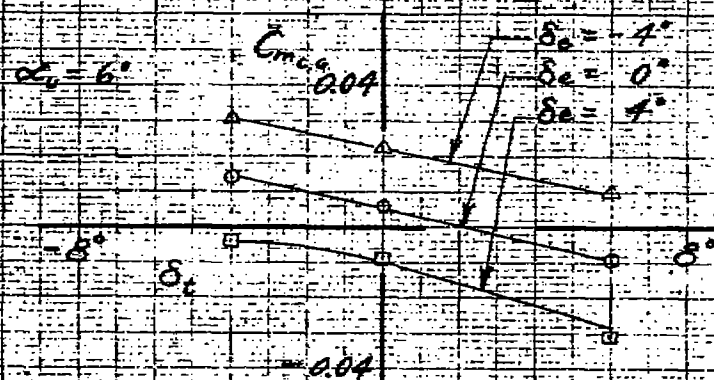
(c) $M = 0.725$

FIGURE 11.- CONTINUED. $\frac{1}{7}$-SCALE YB-49 MODEL.

(d) M = 0.75
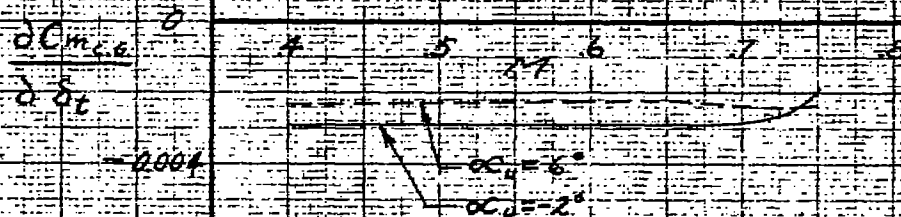
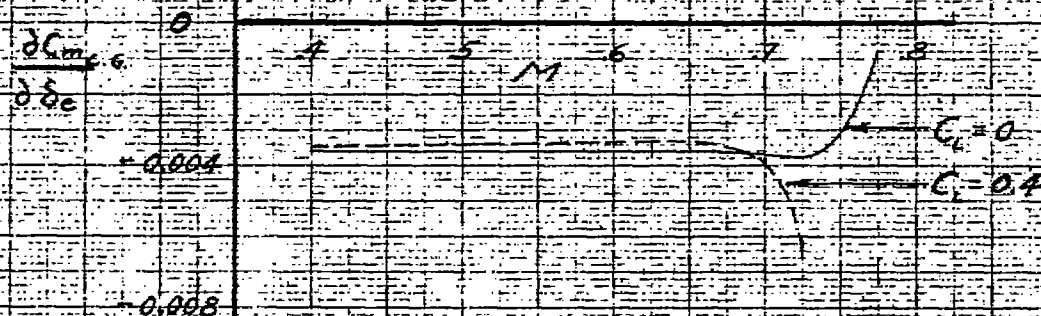FIGURE 11.- CONCLUDED. 1/4-SCALE YB-49 MODEL.

FIGURE 12. — THE EFFECTS OF COMPRESSIBILITY ON THE EFFECTIVENESS OF THE ELEVON AND THE LONGITUDINAL TRIM FLAP. $\frac{1}{7}$-SCALE YB-49 MODEL. $\delta_e = 0°$; $\delta_t = 0°$.

FIGURE 13.- THE VARIATION OF DRAG COEFFICIENT WITH LIFT COEFFICIENT AT SEVERAL MACH NUMBERS. 1/7-SCALE YB-49 MODEL.